Journal of Molecular Catalysis A: Chemical xxx (2014) xxx–xxx

Contents lists available at ScienceDirect

Journal of Molecular Catalysis A: Chemical

journal homepage: www.elsevier.com/locate/molcata

Editor's choice paper

Deactivation and regeneration of Pt/TiO_2 nanosheet-type catalysts with exposed (0 0 1) facets for room temperature oxidation of formaldehyde

Longhui Nie [a,c], Peng Zhou [a], Jiaguo Yu [a,**], Mietek Jaroniec [b,*]

[a] State Key Laboratory of Advanced Technology for Material Synthesis and Processing, Wuhan University of Technology, Luoshi Road 122#, Wuhan 430070, PR China
[b] Department of Chemistry and Biochemistry, Kent State University, Kent, OH 44242, USA
[c] School of Chemistry and Chemical Engineering, Hubei University of Technology, Lijiadun Village 1#, Wuhan 430068, PR China

ARTICLE INFO

Article history:
Received 18 January 2014
Received in revised form 22 February 2014
Accepted 28 February 2014
Available online xxx

Keywords:
Heterogeneous catalysis
Fluorine poisoning
Regeneration
Pt/TiO_2 nanosheets

ABSTRACT

Formaldehyde (HCHO) is a major indoor air pollutant and long-term exposure to HCHO may cause health problems including nasal tumors and skin irritation. Room-temperature catalytic oxidation decomposition of HCHO is considered as the most promising strategy for the removal of HCHO due to its environmental-friendly reaction conditions and energy-saving consideration. In this work, surface-fluorinated anatase TiO_2 nanosheets with dominant {0 0 1} facets ($FTiO_2$-NS) were first prepared by a hydrothermal method using $Ti(OC_4H_9)_4$ and HF as precursors. Then, $Pt/FTiO_2$-NS catalyst with 0.5 wt% Pt loadings was obtained by a combined NaOH-assisted impregnation of titania with Pt precursor and $NaBH_4$-reduction route. The catalytic activity was evaluated by catalytic oxidation decomposition of HCHO vapor at room temperature. Fluoride poisoning (F-poisoning) phenomenon of $Pt/FTiO_2$-NS was first observed for oxidative decomposition of HCHO. The mechanism of F-poisoning is mainly due to blocking of Pt catalytic active sites by strong interactions between Pt and highly electronegative F. In order to recover the catalytic performance, a simple regeneration method for the deactivated $Pt/FTiO_2$-NS catalysts was proposed by NaOH washing.

1. Introduction

Formaldehyde is one of major indoor air pollutants. A long-term exposure to HCHO may cause health problems such as nasal tumors and skin irritation [1]. Room temperature catalytic oxidative decomposition of HCHO to CO_2 and H_2O is considered to be the most promising strategy for removal of HCHO because this process is environmentally friendly and energy saving [2–6]. It overcomes disadvantages of the relatively short lifetime of adsorbents [7–10] and additional instrumentation and operating costs for high-temperature catalytic [11] and photocatalytic oxidation [12,13]. In the case of catalytic oxidation, a variety of supported noble metals like Pt, Pd, and Au [2–6,14–16] were used as catalysts for HCHO oxidation. Among them, the Pt-supported catalysts exhibited an excellent catalytic performance for decomposition of HCHO even at room temperature. For instance, HCHO can be completely oxidized into CO_2 and H_2O on Pt/TiO_2 catalysts at room temperature [2–6,15,17].

However, a major disadvantage of Pt/TiO_2 and related catalysts is their deactivation/poisoning. Therefore, there is a great interest in the basic research devoted to the deactivation and regeneration of Pt/TiO_2 catalysts. While chloride, sulfur, SO_2 and CO poisoning/deactivation of the Pt-supported catalysts were studied in relation to ethane oxidation, fuel cells reactions and hydrogen dissociation reactions [18–20]. Chlorine poisoning for the oxidation activity of supported noble metal catalysts has been investigated by several groups [18,21–24]. For example, Marceau and his coworkers [21,22] reported that residual chlorine ions on Pt/Al_2O_3 catalyst would inhibit the oxidation of methane and the elimination of Cl from catalyst led to higher activity. The poisoning effect of the residual chlorine ions was also observed on the supported Pd catalysts. Simone et al. [23] found that the existence of Cl on the Pd/Al_2O_3 reduced the activity of methane oxidation, and the removal of Cl from catalyst could increase the catalyst's activity. Roth et al. [24]

* Corresponding author at: Kent State University, Department of Chemistry and Biochemistry, Kent, OH 44224, USA. Tel.: +1 3306723790.
** Corresponding author at: Wuhan University of Technology, State Key Laboratory of Advanced Technology for Material Synthesis and Processing, Wuhan 430070, P. R. China. Tel.: +86-27-87871029.
E-mail addresses: jiaguoyu@yahoo.com (J. Yu), jaroniec@kent.edu (M. Jaroniec).

http://dx.doi.org/10.1016/j.molcata.2014.02.033
1381-1169/

Table 1
Experimental conditions for the as-synthesized catalysts and their physical properties.

Sample	Sample composition	Pt dispersion (%)	S_{BET} (m^2/g)	V_{pore} (cm^3/g)	d_{pore} (nm)
A	Pt/FTiO$_2$-NS	6.3	92	0.33	14.3
B	A + NaOH	53.7	87	0.27	12.1
C	Pt/TiO$_2$-NS	66.9	91	0.27	12.1
D	C + HF	9.0	93	0.24	9.4

also confirmed that the presence of Cl on Pd/Al_2O_3 catalyst strongly inhibited the conversion of methane and removal of Cl resulted in the similar activity as Cl-free Pd catalysts. They explained that the observed reduction in the catalytic activity of Pd/Al_2O_3 was caused by partial blocking of Pd surface active sites by the residual chlorine during the aforementioned reaction. Gracia et al. [18] investigated the poisoning effect of Cl of supported Pt catalysts for CO, methane and ethane oxidation in details by in situ IR and controlled atmosphere EXAFS spectroscopy, and they also proposed that site blocking is the mechanism of chloride poisoning. However, fluorine and chlorine are in the same group of periodic table of elements, they have similar chemical properties. Would the fluorine poisoning be happened if supported Pt catalyst is prepared from F-containing precursors or the supports contain F^- ion. To the best of our knowledge, the F-poisoning/deactivation of Pt/TiO_2 catalysts has not been reported yet.

In this paper, F-poisoning/deactivation phenomenon is for the first time reported for a Pt/TiO_2-NS catalyst during the HCHO oxidative decomposition at room temperature, and an efficient regeneration method of the deactivated catalysts is proposed by NaOH washing due to the residual fluorine easily removed from TiO_2 surface [25–27]. The mechanism of fluorine poisoning and regenerated was also discussed.

2. Experimental

2.1. Sample preparation

All reagents were of analytical grade and were used without further purification. Anatase TiO_2 nanosheets with exposed (0 0 1) facets (FTiO$_2$-NS, containing fluoride) were prepared by the hydrothermal method [28,29]. In the typical synthesis, 25 mL of Ti(OC_4H_9)$_4$ and 3 mL of hydrofluoric acid solution (with a concentration ca. 40 wt %) were mixed in a dried Teflon-line autoclave having capacity of 100 mL at ambient temperature, followed by hydrothermal treatment of the mixture at 180 °C for 24 h. After hydrothermal reaction, the white precipitate was collected by centrifuge, washed three times with distilled water and ethanol, and then dried in an oven at 80 °C for 6 h.

A sample of the F-poisoned/deactivated Pt/FTiO$_2$-NS catalyst (denoted as A) was prepared by impregnation of the as-prepared FTiO$_2$-NS with Pt precursor followed by reduction with $NaBH_4$ [30,31]. In a typical preparation, 1 g of FTiO$_2$-NS was added into an H_2PtCl_6 solution (10 mL, 2.56 mmol/L) under magnetic stirring. After impregnation for 1 h, 2.5 mL of the mixed solution of $NaBH_4$ solution (0.1 mol/L) and NaOH solution (0.5 mol/L) was quickly added into the suspension under vigorous stirring for 30 min. After reduction, the suspension was evaporated at 100 °C under stirring. Finally, the samples were dried at 80 °C for 6 h. The nominal weight ratio of Pt to TiO_2 was fixed to be 0.5 wt%. Then, one sample of regenerated Pt/TiO_2-NS catalyst (denoted as B) was obtained by washing the A sample with NaOH solution. In a typical regeneration, 1 g of the sample A was dispersed in 10 mL of 0.5 M NaOH aqueous solution under vigorous shaking for 30 min in an ultrasonic cleaner and then separated. The above process was repeated, and the resulting sample was dried in an oven at 80 °C for 6 h. To investigate F-poisoning deactivation mechanism, a F-free Pt/TiO_2-NS catalyst (sample C) was prepared using F-free TiO_2-NS (F^- was first removed by NaOH solution washing) as the support. F-free TiO_2-NS was obtained by washing twice the sample with 0.5 M NaOH aqueous solution. Then, the sample C was prepared by the above impregnation and $NaBH_4$-reduction method, similarly to the preparation of A. In order to further confirm the effect of fluoride poisoning, the sample C was fluorinated again with HF solution. 0.5 g of sample C was dispersed in 10 mL deionized water, and 0.5 mL HF solution (with a concentration ca. 40 wt%) was added, then stirred for 60 min. Finally, the sample was separated from water and dried in an oven at 80 °C for 6 h; it was denoted as D. The experimental details are shown in Table 1.

2.2. Characterization

Pt/TiO_2-NS catalysts were analyzed using a D/Max-RB X-ray diffractometer (Rigaku, Japan) with Cu K_α radiation at a scan rate (2θ) of 0.05° s^{-1}. Transmission electron microscopy (TEM) and high-resolution transmission electron microscopy (HRTEM) images were collected on a JEM-2100F microscope at an accelerating voltage of 200 kV. X-ray photoelectron spectroscopy (XPS) measurements were performed on VG ESCALAB250xi with X-ray monochromatisation. All binding energies (BE) were referenced to the C 1s peak at 284.8 eV of the surface adventitious carbon. The Brunauer-Emmett-Teller (BET) surface area (S_{BET}) of powders was evaluated from nitrogen adsorption data recorded by using a Micromeritics ASAP 2020 nitrogen adsorption apparatus (USA). All the samples were degassed at 180 °C prior to nitrogen adsorption measurements. The BET surface area was determined by a multipoint method using adsorption data in the relative pressure (P/P_0) range of 0.05–0.3. The pore size distributions were determined using desorption data by the Barrett–Joyner–Halenda (BJH) method. The single-point pore volume was obtained from nitrogen adsorption volume at the relative pressure of 0.98. The relation between the surface area, pore volume and pore width for cylindrical pore model was used to estimate the average value of the latter. Platinum dispersion was measured by H_2 chemisorption on a Micrometrics AutoChem 2920 Pulse Chemisorption System, using a thermal conductivity detector (TCD) to monitor H_2 consumption and assuming a H_2:Pt = 1:2 stoichiometric ratio. Prior to chemisorption, the catalyst was pretreated in flowing argon for 1 h at 200 °C and then it was cooled down to ambient temperature. The chemisorption data were collected stepwise at 45 °C. The platinum dispersion (D) was calculated from the H_2 chemisorption data using the following equation:

$$D = \left(\frac{V_s \times F_s \times M}{W_s \times V_m}\right) \times 100$$

where V_s is the volume of adsorbed gas (STP, standard temperature and pressure) (cm^3), F_s is the stoichiometric factor, which is equal 2 for Pt, W_s is the weight (g) of noble metal Pt, M is the molecular weight of Pt (g/mol) and V_m is the ideal gas molar volume = 22414 (cm^3/mol).

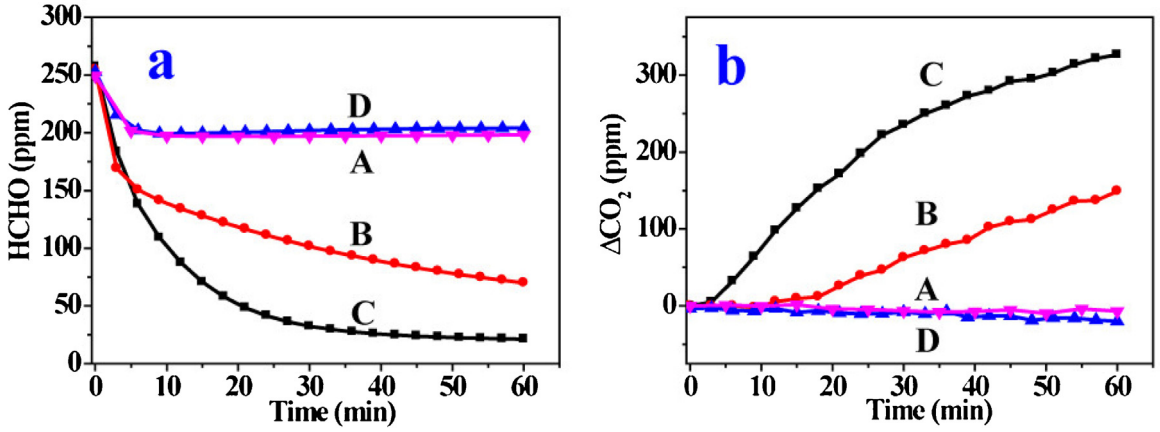

Fig. 1. Changes in formaldehyde concentration (a) and ΔCO_2 (the difference between CO_2 concentration at *t* reaction time and initial time, ppm) (b) as a function of reaction time for the A–D samples.

2.3. Catalytic activity test

The room-temperature catalytic oxidation of HCHO was performed in a dark organic glass box covered by a layer of aluminum foil on its inner wall at 25 °C in the same way as it is reported in our previous work [30,31]. An amount of 0.3 g catalyst was dispersed on the bottom of glass Petri dish with a diameter of 14 cm. After placing the sample-coated dishes in the bottom of reactor with a glass slide cover, 12 μL of condensed HCHO solution (38%) was injected into reactor and a 5 W fan was placed on the bottom of the reactor. After 2 h, the HCHO solution was volatilized completely and the concentration of HCHO was stabilized. The analysis of HCHO and CO_2 was on-line conducted by a Photoacoustic IR Multigas Monitor (INNOVA air Tech Instruments Model 1412). The HCHO vapor was allowed to reach adsorption equilibrium within the reactor prior to catalytic activity experiments. The initial concentration of HCHO after adsorption equilibrium was controlled at about 253 ppm, which remained constant until the glass slide cover on the petri dish was removed to start the catalytic oxidation reaction of HCHO. Each set of experiments was followed for about 60 min. The CO_2 concentration increase (ΔCO_2, which is the difference between CO_2 concentration at *t* reaction time and initial time, ppm) and HCHO concentration decrease was used to evaluate the catalytic performance.

3. Results and discussions

3.1. Catalytic activity

The catalytic performance of F-poisoned/deactivated (A and D), regenerated (B) and F-free (C) catalysts in HCHO oxidation is shown in Fig. 1.

As can be seen from this figure, the HCHO concentration decreased quickly during initial 6 min and then remained almost unchanged in the subsequent 55 min for the F-poisoned/deactivated A and D catalysts. Also, the CO_2 concentration was almost unchanged in the whole process, indicating that HCHO was not decomposed and was mainly adsorbed on the surface of the catalysts. When the F-removed or regenerated catalyst (B) was used for HCHO oxidation, the HCHO concentration decreased with increasing reaction time, and accordingly, the CO_2 concentration increased, indicating oxidation of HCHO into CO_2 and H_2O; thus, the catalytic performance was evaluated. Especially, for the F-free catalyst (C), HCHO concentration decreased more rapidly and CO_2 concentration increased faster with increasing reaction time than in the case of B. The above results imply that the presence of F^- results in the deactivation of the catalyst, which is not beneficial for room temperature oxidative decomposition of HCHO.

In order to investigate the difference in the catalytic performance for HCHO oxidation, the A, B and C samples were characterized by X-ray diffraction (XRD), transmission electron microscopy (TEM), high-resolution transmission electron microscopy (HRTEM), X-ray photoelectron spectroscopy (XPS) and N_2 adsorption-desorption isotherms. The Pt dispersion on the catalysts was determined by pulse H_2 chemisorption.

3.2. Phase structures and morphology

The XRD patterns of the $FTiO_2$-NS, A–C samples are presented in Fig. 2, indicating that the phase structure of the $FTiO_2$-NS samples is anatase (JCPDS, No. 21-1272); also, there is no obvious change in the position and height of TiO_2 diffraction peaks before and after Pt deposition and NaOH washing (for samples A–C). Further observation indicates that no diffraction peaks of Pt are observed in the XRD patterns for the A–C samples due to its low loading (0.5 wt%), small particle size, and good dispersion [30–32].

TEM and HRTEM results are shown in Fig. 3, confirming the presence of TiO_2 nanosheets and Pt nanoparticles (NPs). TEM image (Fig. 3a) of A shows that a large amount of nanosheets with side length of ca. 30–40 nm and the size of Pt NPs on their surface is ca. 4–6 nm. NaOH washing did not affect the size of Pt NPs on B. Contrarily, Pt NPs appear to be aggregated (see Fig. 3b). Surprisingly,

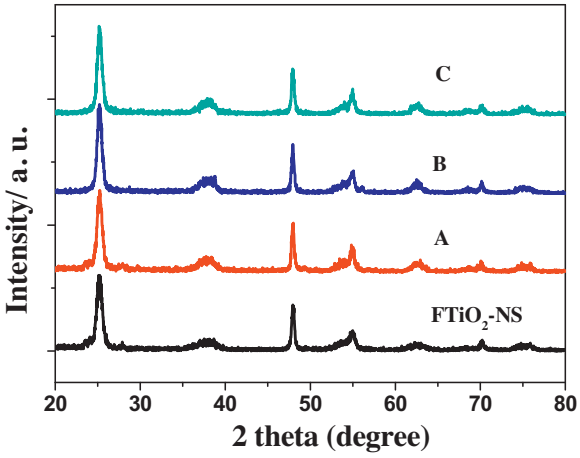

Fig. 2. XRD patterns of the $FTiO_2$-NS, A–C samples.

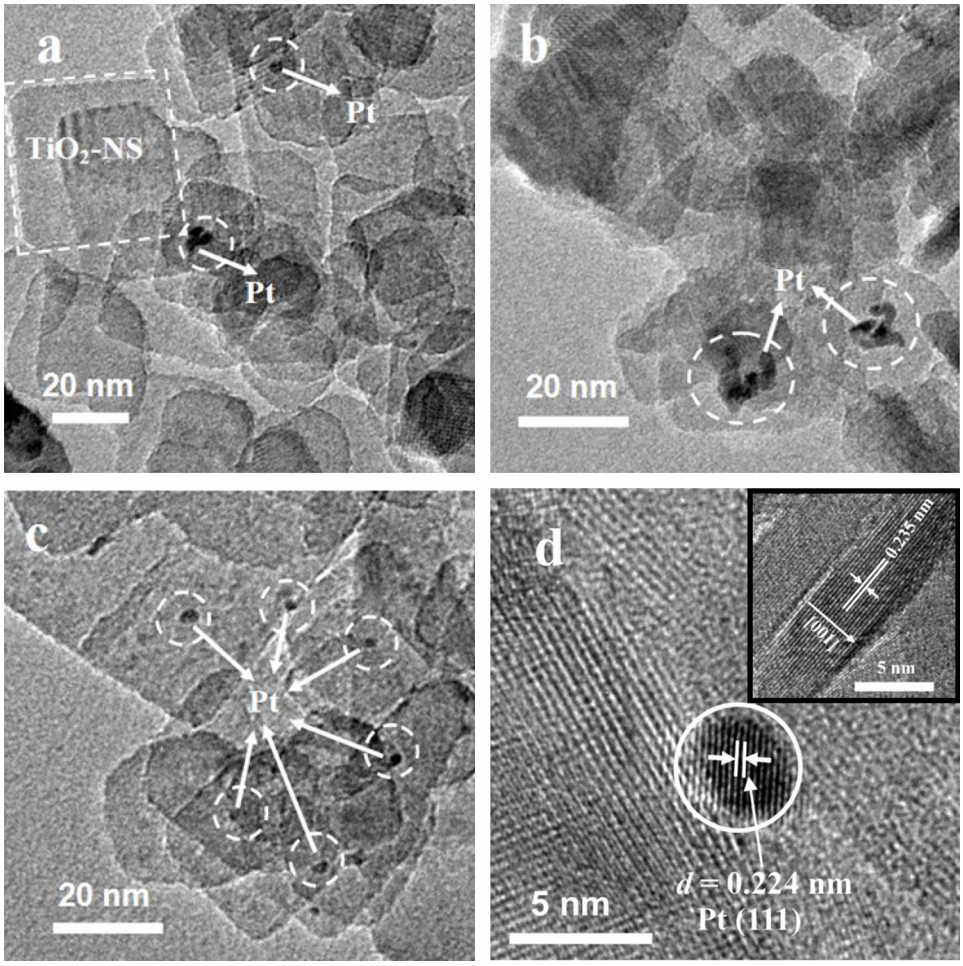

Fig. 3. TEM images (a–c) of the A (a), B (b) and C (c) samples and HRTEM image (d) of the C sample. The inset in the panel (d) shows that the lattice spacing parallel to the top and bottom facets of a nanosheet is ca. 0.235 nm.

the size (around 1–3 nm) of Pt NPs on C is obviously smaller than that on the A and B samples. Also the distribution of Pt NPs on the C sample (Fig. 3c) is more uniform than that on the A and B samples. HRTEM image (Fig. 3d) of black Pt NPs shows that the lattice spacing in white circle is ca. 0.224 nm, which is consistent with the lattice spacing of (1 1 1) plane of metallic Pt, confirming the presence of Pt NPs [33]. The HRTEM image of TiO_2 nanosheet (see the inset of Fig. 3d) indicates that the lattice space parallel to the top and bottom facets is ca. 0.235 nm, corresponding to the (0 0 1) planes of anatase TiO_2, suggesting that the top and bottom facets of the nanosheets are the (0 0 1) and (0 0 −1) planes of anatase TiO_2, respectively. Why smaller Pt NPs are observed in the case of the C sample? One possible explanation is because TiO_2-NS support was first washed with NaOH solution before Pt deposition, which resulted in the removal of F^- and the creation of more hydroxyls on this support [34]. The F-free TiO_2-NS support seems to enhance adsorption of H_2PtCl_6 precursor and deposition of Pt NPs. Therefore, it is not surprising that the C sample showed smaller Pt NPs and more uniformly distributed on the TiO_2-NS surface. It is notable that the smaller Pt NPs are more beneficial for the oxidation of HCHO because they have more active centers than the big Pt NPs.

3.3. BET surface areas and pore size distributions

Nitrogen adsorption-desorption isotherms and the corresponding pore size distribution curves (inset) for the A–C samples are shown in Fig. 4, indicating no obvious difference in the shape of adsorption isotherms and pore size distributions. This result is not surprising because the A–C samples were mainly composed of TiO_2-NS. Table 1 shows also a comparison of the BET specific surface area, pore volume and pore size values for the A–D samples, indicating that there is no significant change in the aforementioned quantities.

3.4. XPS analysis

The chemical state of species present in the prepared samples was investigated by XPS; the high-resolution XPS spectra of F 1s, Pt 4f, Ti 2p and O 1s regions are shown in Fig. 5.

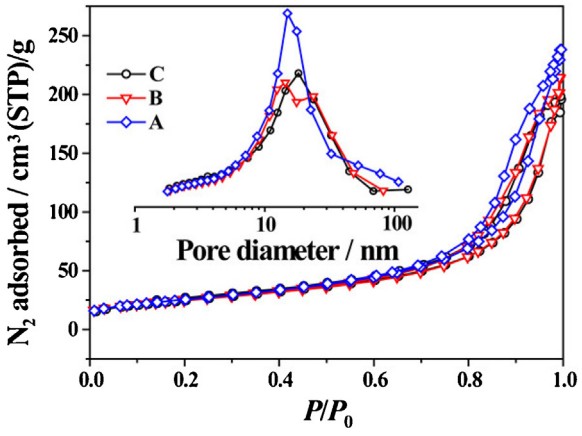

Fig. 4. Nitrogen adsorption–desorption isotherms and the corresponding pore–size distribution curves (inset) for the A–C samples.

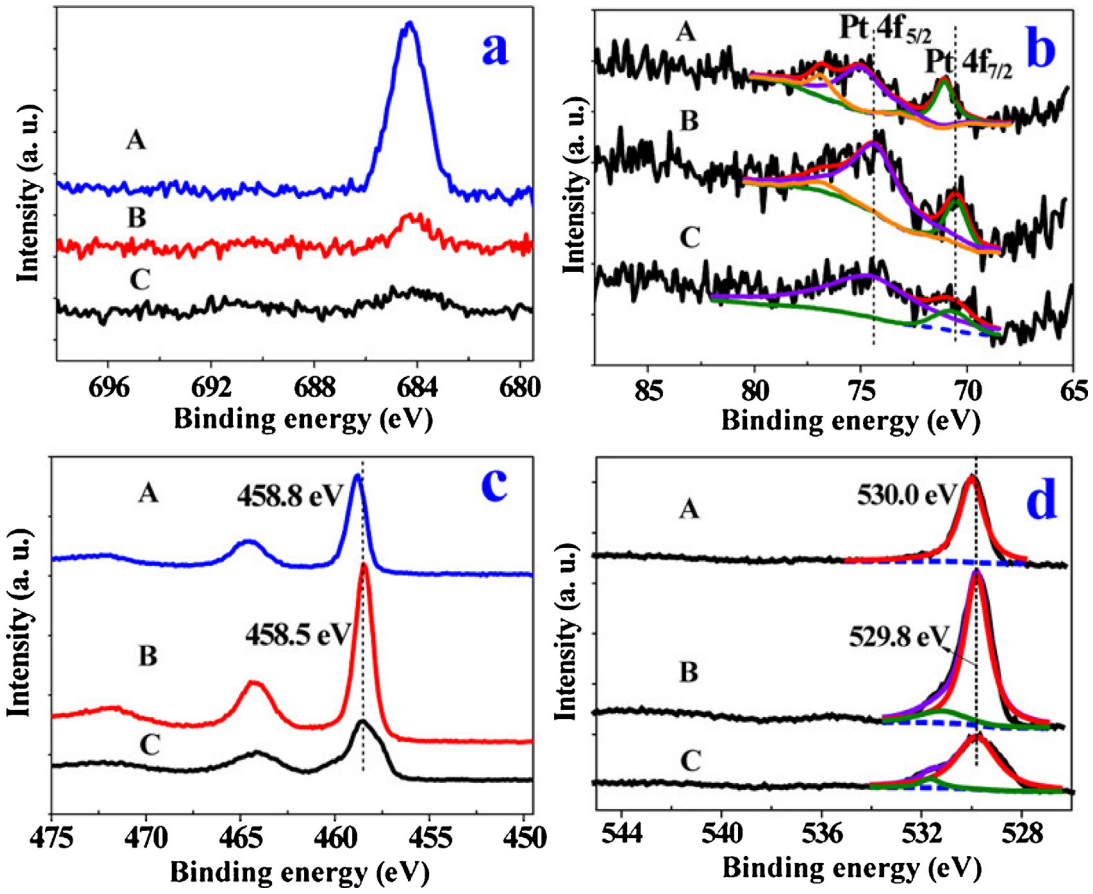

Fig. 5. High-resolution XPS spectra for F 1s (a), Pt 4f (b), Ti 2p (c) and O 1s (d) of the A–C samples.

The high-resolution F 1s spectra of the A–C samples (Fig. 5a) show one peak observed at 684.4 eV, which is a typical value for physically absorbed F^- on the surface of TiO_2 (≡Ti–F). No signal for F^- in the lattice of TiO_2 (binding energy = 688.5 eV) was found. After NaOH washing of A, the F 1s signal of the B sample decreased significantly, implying that the most of F^- was removed from the TiO_2 surface. Note that the lowest F concentration was in the case of C, which exhibited the best catalytic activity. This result clearly indicates that the presence of F^- results in the poisoning/deactivation of Pt/TiO_2-NS catalysts.

The high-resolution Pt 4f spectra of the B and C samples (Fig. 5b) show two peaks at ca. 70.5 eV and 74.3 eV, which are assigned to Pt $4f_{7/2}$ and Pt $4f_{5/2}$ of metallic Pt, respectively. It is known that the Pt $4f_{7/2}$ binding energy of Pt^0 is around 71.2 eV. A negative shift for Pt $4f_{7/2}$ is observed as compared to the binding energy of Pt $4f_{7/2}$ for bulk metallic Pt^0 (71.2 eV) [35,36], which can be caused by the electron transfer from TiO_2 to Pt (see Fig. 6a) due to strong metal-support interactions (SMSI) [5,30].

Further observation indicates that the Pt $4f_{7/2}$ peak of the A sample exhibits an obvious positive shift as compared to that of the B and C samples. Also, the Pt $4f_{5/2}$ peak of the A sample (Fig. 5b) shows one extra peak at ca. 76.8 eV, which can be due to the adsorption of F^- on the surface of Pt NPs and the formation of Pt–F bond, leading to the transfer of electrons from Pt to highly electronegative F [36]. How the Pt–F bond is formed? One possible explanation is that during the preparation of the A sample, partial F^- on the TiO_2 surface can be removed by a exchange reaction between Ti–F and OH^- due to the addition of NaOH (see Eq. (1)) [37–39].

$$\equiv Ti\text{–}F + OH^- \rightarrow \equiv Ti\text{–}OH + F^- \quad (1)$$

Thus, it is not surprising that the produced free F^- can easily adsorb the surface of the as-prepared Pt NPs, resulting in the formation of Pt–F bond, and F-poisoning and deactivation of Pt NPs. The above XPS result also suggests that the interaction between F and Pt is stronger than the interaction between F and Ti in basic solution. A positive shift in the binding energies of Ti 2p and O 1s is also observed for the A sample (see Fig. 5c and d) because F induces a consecutive electron transfer, first from Pt to F, then from O to Pt and finally from Ti to O (see Fig. 6b). Thus, the XPS analysis shows that the F poisoning/deactivation of Pt/TiO_2-NS catalysts is due to the adsorption of F^- on Pt NPs.

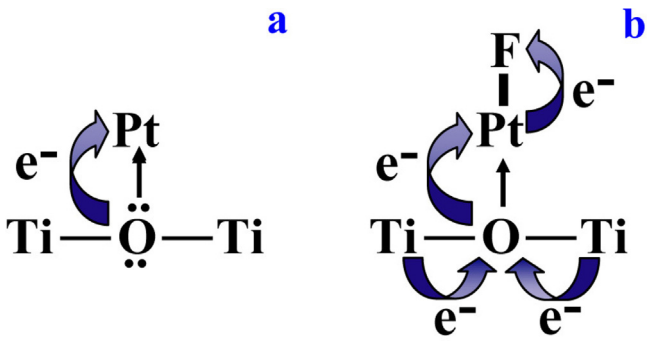

Fig. 6. Schematic diagram of electron transfer between Pt and TiO_2 for the B and C samples (a) and the transfer between F, Pt, O and Ti elements present in the A sample (b).

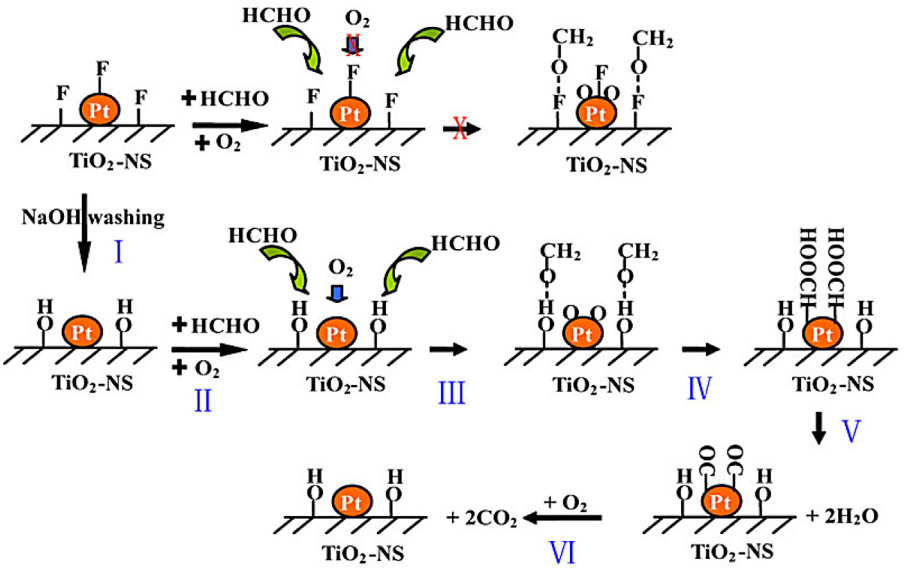

Fig. 7. Proposed F-poisoning/deactivation mechanism and regeneration by NaOH washing for the oxidative decomposition of HCHO on Pt/TiO_2-NS.

3.5. Deactivation mechanism and regeneration analysis

The room temperature catalytic oxidative decomposition of HCHO on Pt/TiO_2 takes place because HCHO and O_2 are first adsorbed onto TiO_2 and Pt surface (see step II in Fig. 7), respectively.

Next, O_2 becomes an active oxygen (step III), which is very important stage in the oxidation of HCHO. After that, HCHO is oxidized into formate species on the surface (step IV) and these species are decomposed into adsorbed CO species and H_2O (step V); finally, CO species react with O_2 to generate gaseous CO_2 (step VI). Because of strong interactions between Pt and F on the surface of A, the formation of active oxygen species is difficult due to the site blocking effect (see the top part of Fig. 7), which is similar to the site blocking effect in the case of Cl on Pt NPs [18]; thus, HCHO oxidation is inhibited. The site blocking effect for F^- was also verified by measurement of Pt dispersion on the samples using H_2 chemisorption. After F-poisoning/deactivation, the Pt dispersion on the A and D samples is 6.3% and 9.0% (see Table 1), respectively, which is much smaller than that (53.7 and 66.9%) on the B and C samples. So, no HCHO oxidation activity is observed on the A and D samples due to the F-poisoning/deactivation of the Pt NPs (see Fig. 1).

In order to eliminate the effect of F-poisoning in the case of Pt/TiO_2-NS catalysts, two regeneration methods were investigated for the F^- removal. The previous investigations indicated that F^- on TiO_2-NS can be almost completely removed by NaOH solution washing in a strong basic environment [25–27]. Therefore, it is not surprising that the C sample exhibited the highest catalytic activity because F^- was fully removed from TiO_2-NS by NaOH washing and the C sample has the smallest Pt NPs on its surface. Of course, the smaller the Pt NPs, the higher their catalytic activity is. Also, the NaOH washing was powerful for regeneration of the F-poisoned/deactivated A sample to obtain B (see step I in Fig. 7). So, the latter showed very good catalytic activity for HCHO decomposition. Fig. 1 also indicates that the C sample exhibited higher catalytic activity than the B sample, which is not surprising because the former contained much less F^- (see Fig. 5a) and the smaller Pt NPs; thus, the removal of F^- can be easier from FTiO_2-NS than from Pt/FTiO_2-NS. The previous XPS studies also indicate that the interaction between F and Pt is stronger than the interaction between F and Ti in basic solution, implying that a small amount of F^- could be still present in the B sample, which partly resulted in its lower catalytic activity.

4. Conclusions

In summary, F-poisoning/deactivation mechanism is explained for Pt/TiO_2-NS catalysts used in the oxidative decomposition of HCHO at room temperature. Also, an effective and simple regeneration is proposed for F-poisoned Pt/FTiO_2-NS catalysts. This study shows that the site blocking effect for F on Pt catalysts (F-poisoning) is responsible for inhibition of O_2 adsorption and for production of active oxygen species. The F-poisoned/deactivated Pt/TiO_2-NS catalysts can be effectively regenerated by NaOH washing, which removes the most of F^- and recovers the catalytic activity of Pt/TiO_2-NS. Due to the importance and diversity of noble-metal Pt catalysts, the proposed site-blocking mechanism of F-poisoning/deactivation and effective regeneration of these catalysts represent an important contribution to the development of high-performance noble metal catalysts for indoor air purification.

Acknowledgments

This work was supported by the 863 Program (2012AA062701), 973 Program (2013CB632402), NSFC (21177100, 51272199, 51320105001 and 51372190), National Science Fund for Postdoctoral Scientists of China (2012M511292), Fundamental Research Funds for the Central Universities (WUT: 2013-VII-030) and Self-determined and Innovative Research Funds of SKLWUT (2013-ZD-1 and 2013-KF-10).

References

[1] J.J. Collins, R. Ness, R.W. Tyl, N. Krivanek, N.A. Esmen, T.A. Hall, Regul. Toxicol. Pharm. 34 (2001) 17–34.
[2] C.B. Zhang, H. He, K. Tanaka, Catal. Commun. 6 (2005) 211–214.
[3] C.B. Zhang, H. He, K. Tanaka, Appl. Catal., B 65 (2006) 37–43.
[4] C.B. Zhang, F.D. Liu, Y.P. Zhai, H. Ariga, N. Yi, Y.C. Liu, K. Asakura, M. Flytzani-Stephanopoulos, H. He, Angew. Chem. Int. Ed. 51 (2012) 9628–9632.
[5] H.B. Huang, D.Y.C. Leung, J. Catal. 280 (2011) 60–67.
[6] H.B. Huang, D.Y.C. Leung, D. Ye, J. Mater. Chem. 21 (2011) 9647–9652.
[7] Z.H. Xu, J.G. Yu, G. Liu, B. Cheng, P. Zhou, X.Y. Li, Dalton Trans. 42 (2013) 10190–10197.
[8] Z.H. Xu, J.G. Yu, W. Xiao, Chem. Eur. J. 19 (2013) 9592–9598.
[9] Y. Le, D.P. Guo, B. Cheng, J.G. Yu, Appl. Surf. Sci. 274 (2013) 110–116.
[10] P. Zhou, X.F. Zhu, J.G. Yu, W. Xiao, ACS Appl. Mater. Interfaces 5 (2013) 8165–8172.
[11] S. Scirè, S. Minicò, C. Crisafulli, C. Satriano, A. Pistone, Appl. Catal., B 40 (2003) 43–49.

[12] R.C.W. Lama, M.K.H. Leung, D.Y.C. Leung, L.L.P. Vrijmoedb, W.C. Yamc, S.P. Ng, Sol. Energy Mater. Sol. Cells 91 (2007) 54–61.
[13] J.G. Yu, S.H. Wang, J.X. Low, W. Xiao, Phys. Chem. Chem. Phys. 15 (2013) 16883–16890.
[14] H.B. Huang, D.Y.C. Leung, ACS Catal. 1 (2011) 348–354.
[15] C.B. Zhang, H. He, Catal. Today 126 (2007) 345–350.
[16] D. Chen, Z.P. Qu, S.J. Shen, X.Y. Li, Y. Shi, Y. Wang, Q. Fu, J.J. Wu, Catal. Today 175 (2011) 338–345.
[17] X.F. Tang, J.L. Chen, X.M. Huang, Y.D. Xu, W.J. Shen, Appl. Catal., B 81 (2008) 115–121.
[18] F.J. Gracia, J.T. Miller, A.J. Kropf, E.E. Wolf, J. Catal. 209 (2002) 341–354.
[19] P. Trens, R. Durand, B. Coq, C. Coutanceau, S. Rousseau, C. Lamy, Appl. Catal., B 92 (2009) 280–284.
[20] F. Xie, Z.G. Shao, G. Zhang, J. Zhai, W. Lu, X. Qin, W. Lin, B. Yi, Electrochim. Acta 67 (2012) 50–54.
[21] E. Marceau, M. Che, J. Saint-Just, J.M. Tatibouet, Catal. Today 29 (1996) 415–419.
[22] E. Marceau, H. Lauron-Pernot, M. Che, J. Catal. 197 (2001) 394–405.
[23] D.O. Simone, T. Kennelly, N.L. Brungard, R.J. Farrauto, Appl. Catal. 70 (1991) 87–100.
[24] D. Roth, P. Gelin, M. Primet, E. Tena, Appl. Catal., A 203 (2000) 37–45.
[25] M. Minella, M.G. Faga, V. Maurino, C. Minero, E. Pelizzetti, S. Coluccia, G. Martra, Langmuir 26 (2010) 2521–2527.
[26] S.W. Liu, J.G. Yu, B. Cheng, M. Jaroniec, Adv. Colloid Interface Sci. 173 (2012) 35–53.
[27] S.W. Liu, J.G. Yu, M. Jaroniec, Chem. Mater. 23 (2011) 4085–4093.
[28] Q.J. Xiang, K.L. Lv, J.G. Yu, Appl. Catal., B 96 (2010) 557–564.
[29] Q.J. Xiang, J.G. Yu, M. Jaroniec, Nanoscale 3 (2011) 3670–3678.
[30] L.H. Nie, J.G. Yu, X.Y. Li, G. Liu, M. Jaroniec, Environ. Sci. Technol. 47 (2013) 2777–2783.
[31] L.H. Nie, A.Y. Meng, J.G. Yu, M. Jaroniec, Sci. Rep. 3 (2013) 3215.
[32] J.X. Peng, S.D. Wang, Appl. Catal., B 73 (2007) 282–291.
[33] N. Shang, P. Papakonstantinou, P. Wang, S. Ravi, P. Silva, J. Phys. Chem. C 114 (2010) 15837–15841.
[34] J.G. Yu, X.Y. Li, Z.H. Xu, W. Xiao, Environ. Sci. Technol. 47 (2013) 9928–9933.
[35] K.D. Schierbaum, S. Fischer, M.C. Torquemada, J.L. de Segovis, E. Roman, J.A. Martin-Gago, Surf. Sci. 345 (1996) 261–273.
[36] J.F. Moulder, W.F. Stickle, P.E. Sobol, K.D. Bomben, J. Chastain (Eds.), Handbook of X-Ray Photoelectron Spectroscopy, Pekin-Elmer Inc. Physical Electronics Division, Eden Prairie, MN, 1992.
[37] C. Minero, G. Mariella, V. Maurino, E. Pelizzetti, Langmuir 16 (2000) 2632–2641.
[38] M.S. Vohra, S. Kim, W. Choi, J. Photochem. Photobiol., A 160 (2003) 55–56.
[39] K.L. Lv, B. Cheng, J.G. Yu, G. Liu, Phys. Chem. Chem. Phys. 14 (2012) 5349–5362.

Please cite this article in press as: L. Nie, et al., J. Mol. Catal. A: Chem. (2014), http://dx.doi.org/10.1016/j.molcata.2014.02.033